Pressure-driven transformation of the ordering in amorphous network-forming materials

Anita Zeidler and Philip S. Salmon
Department of Physics, University of Bath, Bath, BA2 7AY, United Kingdom
(Received 2 September 2015; revised manuscript received 29 March 2016; published 22 June 2016)

The pressure-induced changes to the structure of disordered oxide and chalcogenide network-forming materials are investigated on the length scales associated with the first three peaks in measured diffraction patterns. The density dependence of a given peak position does not yield the network dimensionality, in contrast to metallic glasses where the results indicate a fractal geometry with a local dimensionality of $\simeq 5/2$. For oxides, a common relation is found between the intermediate-range ordering, as described by the position of the first sharp diffraction peak, and the oxygen-packing fraction, a parameter that plays a key role in driving changes to the coordination number of local motifs. The first sharp diffraction peak can therefore be used to gauge when topological changes are likely to occur, events that transform network structures and their related physical properties.

DOI: 10.1103/PhysRevB.93.214204

I. INTRODUCTION

Network structures govern the physicochemical characteristics of a broad class of glassy and liquid materials, and can be altered profoundly by changing the state conditions [1–5]. Here, essential information on the structure is provided by diffraction, and it is therefore desirable to link generic features in the structure factor $S(k)$ measured by experiment, where k denotes the magnitude of the scattering vector, to the character of network-forming motifs, and to the way in which these motifs are organized [6–16]. In this quest, the bulk number density ρ is a key parameter that depends on the nature of the interatomic interactions, is a prerequisite for building accurate atomic-scale models, and can be manipulated by changing the pressure. There has not, however, been a systematic investigation of the density dependence of the rudimentary features in $S(k)$ for network-forming materials.

At ambient conditions, the open network structures of oxide and chalcogenide glass-forming materials often lead to $S(k)$ functions that are characterized by three peaks with positions k_i ($i = 1$, 2, or 3) that scale roughly with the interatomic distance d such that $k_1 d \simeq 2$–3, $k_2 d \simeq 4.6$–4.9, and $k_3 d \simeq 7.7$–8.9 [6–10,15] (Fig. 1). According to Fourier transform theory, each feature corresponds to real-space ordering with a periodicity of $2\pi/k_i$ and a correlation length of $2\pi/\Delta k_i$, where Δk_i is the peak width [10]. The peaks are associated with ordering on length scales that are commensurate with the nearest-neighbor separations (k_3), with the size of the local network-forming motifs (k_2), and with the arrangement of these motifs on an intermediate range (k_1). The features at k_2 and k_1 are commonly referred to as the principal peak and first sharp diffraction peak (FSDP), respectively, and the real-space periodicity associated with these features is directly observable for several network-forming materials [10,12,15,17]. The finding $k_3 d \simeq 7.7$–8.9 is roughly in keeping with the Ehrenfest relation $k_3 d = 7.725$ [10].

In contrast to their network-forming counterparts, the local motifs in metallic glasses are closely packed to favor an efficient filling of space [11,13,18]. In this case, $S(k)$ is dominated by a first peak at a scaled peak position $k_3 d \simeq 7$–8 [7] (Fig. 1), and the associated real-space periodicity is directly observable for many of these materials [14,19]. Recent experiments in which pressure was used as a parameter to tune the density found a "universal" fractional power-law relation $k_3 \propto \rho^{1/D_3}$ with $D_3 \simeq 5/2$ [16], similar to the value of $D_3 \simeq 2.31$ found from an investigation in which composition was used as a tuning parameter [14]. These findings are at odds with an often assumed $D_3 = 3$ dependence, i.e., with an expectation that the density under compression should vary in inverse proportion to the cube of the one-dimensional interatomic distance, and it is proposed that the motifs pack to give a fractal geometry with a local dimensionality of $\simeq 5/2$ [14,16,20]. As pointed out by Zeng *et al.* [16], it is unknown whether this type of behavior is also observed for other classes of amorphous material. We have therefore been motivated to examine the density dependence of the peak positions in $S(k)$ for network glass-forming oxide and chalcogenide systems at high pressures. Under ambient conditions, these systems cover a range in network dimensionality from, e.g., 1-D for amorphous Se to 3-D for amorphous SiO_2 [21].

The paper is organized as follows. In Sec. II, we consider the reduced density dependence of the peak positions in $S(k)$ for network-forming versus metallic glasses, where the peak positions are categorized as according to Fig. 1. In general, a given peak position k_i is not found to share a common density dependence for a given class of network-forming materials, and does not provide a direct measure of the network dimensionality. In Sec. III, we investigate whether the oxygen-packing fraction η_O provides an alternative parameter for rationalizing the high-pressure diffraction results for amorphous oxides. This parameter is chosen because it plays a key role in facilitating the pressure-driven changes to the connectivity of network-forming motifs [4]. Here, a relationship is found between η_O and the intermediate-range ordering as described by k_1, which also holds for the available data for molten oxides at high-pressure and high-temperature conditions. The implications of this relationship are discussed in terms of predicting when network transformations are likely to occur. Conclusions are drawn in Sec. IV.

II. NETWORK DIMENSIONALITY

Figure 2(a) shows the reduced density ρ/ρ^0 dependence of the scaled peak position k_3/k_3^0, where superscripts refer to ambient pressure parameters, as obtained from *in situ* high-pressure x-ray and neutron diffraction experiments on

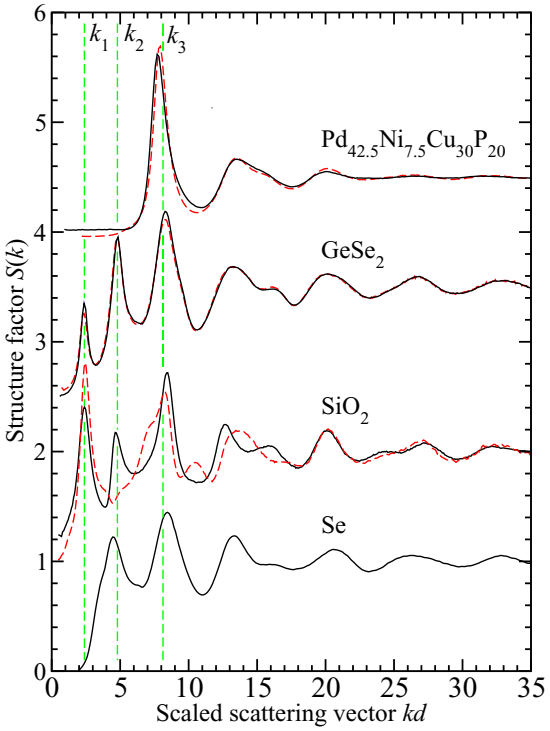

FIG. 1. Representative structure factors $S(k)$, as measured at ambient pressure by neutron diffraction (ND) [solid curves] or x-ray diffraction (XRD) [broken (red) curves] and plotted in terms of the scaled scattering vector kd, for a bulk-metallic glass $Pd_{42.5}Ni_{7.5}Cu_{30}P_{20}$ [$d = 2.656$ Å (ND) or $d = 2.739$ Å (XRD)], for a network-forming chalcogenide glass $GeSe_2$ ($d = 2.363$ Å), for a network-forming oxide glass SiO_2 ($d = 1.599$ Å), and for elemental glassy Se ($d = 2.349$ Å). The ND and XRD $S(k)$ functions for $GeSe_2$ and the ND $S(k)$ function for SiO_2 show a "three-peak" structure that is typical of network-forming materials, where the approximate positions of these peaks as labeled by k_1, k_2, and k_3 are indicated by the vertical broken lines. A principal peak at k_2 is absent in the XRD $S(k)$ function for SiO_2 (see the text). For the metallic glass, ordering does not appear on a length scale associated with either k_1 or k_2 and the magnitude of $S(k)$ has been halved for clarity of presentation. For Se, ordering does not appear on a length scale associated with k_1.

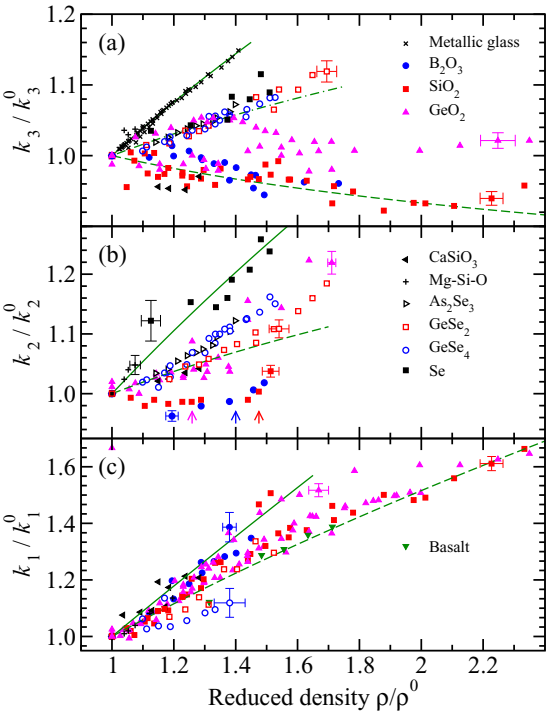

FIG. 2. The reduced density ρ/ρ^0 dependence of the scaled (a) peak position k_3/k_3^0, (b) principal peak position k_2/k_2^0, and (c) FSDP position k_1/k_1^0 as measured by using *in situ* high-pressure x-ray or neutron diffraction for materials under compression. In (a) the solid curve corresponds to $D_3 = 5/2$ and accounts for the metallic glass data taken from Refs. [16,23], and the chained and broken curves correspond to D_3 values of 6 and -10, respectively. In (b) the solid curve corresponds to $D_2 = 1.82$, and the broken curve corresponds to $D_2 = 5$. The vertical arrows indicate (from left to right) the reduced densities at which the coordination number $\bar{n}_{AO}$ of the local motifs in glassy GeO_2, B_2O_3, and SiO_2 starts to exceed its ambient pressure value of 4, 3, or 4, respectively. In (c) the solid and broken curves correspond to D_1 values of 10/9 and 5/3, respectively, and bracket most of the measured data points. The horizontal and vertical error bars on several of the data points give representative uncertainties.

different amorphous materials under compression at ambient temperature. In these experiments the structure factor is defined by [22]

$$S(k) \equiv \sum_{\alpha}\sum_{\beta} w_{\alpha\beta}(k) S_{\alpha\beta}(k), \qquad (1)$$

i.e., there is a weighted overlap of partial structure factors $S_{\alpha\beta}(k)$ where $w_{\alpha\beta}(k) = c_\alpha c_\beta f_\alpha(k) f_\beta^*(k)/|\langle f(k)\rangle|^2$, c_α and $f_\alpha(k)$ are the atomic fraction and x-ray form factor (or coherent neutron scattering length) for chemical species α, respectively, and $\langle f(k)\rangle = \sum_\alpha c_\alpha f_\alpha(k)$ is the mean form factor. The data sets correspond to the bulk metallic glasses $La_{62}Al_{14}Cu_{11.7}Ag_{2.3}Ni_5Co_5$, $La_{62}Al_{14}Co_{10.83}Ni_{10.83}Ag_{2.34}$, $Cu_{47}Ti_{33}Zr_{11}Ni_8Nb_1$, and $Ce_{68}Al_{10}Cu_{20}Co_2$ [16,23], the network-forming oxide glasses B_2O_3 [24,25], SiO_2 [26–29], and GeO_2 [30–35], the modified oxide glasses $CaSiO_3$ [36] and $(MgO)_{0.62}(SiO_2)_{0.38}$ [37], the network-forming chalcogenide glasses $GeSe_2$ [38,39], $GeSe_4$ [40–42], and As_2Se_3 [36], and elemental glassy Se [43–46]. For each chalcogenide glass, the measured x-ray and neutron $S(k)$ functions are comparable because of a similarity in the relative weighting factors $w_{\alpha\beta}(k)$ [5,15].

In Fig. 2(a), the data sets for the metallic glasses sit on a common curve given by $k_3/k_3^0 = (\rho/\rho^0)^{1/D_3}$ with $D_3 = 5/2$ [16], which provides a bound on the reduced density dependence of k_3/k_3^0 for most of the other materials. The data sets for the chalcogenides cluster together and indicate an initial power-law dependence for k_3 with $D_3 \sim 6$ which does not, however, correspond to a meaningful network dimensionality. The data sets for the oxides are bracketed by curves corresponding to maximum and minimum D_3 values of $\sim$6 and ~ -10, respectively.

Figure 2(b) shows the reduced-density dependence of the scaled principal peak position k_2/k_2^0 for the same set of materials as shown in Fig. 2(a), except that data for the metallic glasses are missing because ordering does not occur on a length scale associated with k_2 (Fig. 1). In the case of oxides,

a principal peak is not always present in the $S(k)$ function measured by both x-ray and neutron diffraction, even when this feature is prominent in the partial structure factors $S_{\alpha\beta}(k)$, on account of the weighting factors $w_{\alpha\beta}(k)$ in Eq. (1). For instance, a principal peak is present in the neutron diffraction $S(k)$ but not in the x-ray diffraction $S(k)$ for glassy SiO_2 (Fig. 1) because there is a cancellation in the latter of the principal peaks in $S_{SiSi}(k)$ and $S_{OO}(k)$ with a principal trough in $S_{SiO}(k)$ [47]. The data sets for SiO_2 [29] and B_2O_3 [24] are therefore taken from neutron and x-ray diffraction, respectively. The other data sets in Fig. 2(b) correspond to GeO_2 [31–34], $CaSiO_3$ [36], $(MgO)_{0.62}(SiO_2)_{0.38}$ [37], $GeSe_2$ [38,39], $GeSe_4$ [40–42], and As_2Se_3 [36].

In Fig. 2(b), the data sets for the chalcogenide glasses indicate a power-law dependence $k_2/k_2^0 = (\rho/\rho^0)^{1/D_2}$ with D_2 values of 1.82(8), 3.13(5), 3.65(6), and 4.4(2) for Se, $GeSe_4$, As_2Se_3, and $GeSe_2$, respectively. Here, the ambient-pressure network dimensionality is 1-D for Se, where the structure is formed from Se_n chains (n is an integer $\geqslant 2$); increases in the order from $GeSe_4$ to $GeSe_2$, as the added Ge atoms form more cross-links between Se_n chains, to give a dimensionality $\leqslant 3$ for $GeSe_2$; and is 2-D for As_2Se_3, where $AsSe_3$ pyramids link to form layer-like arrangements [21,48]. There may therefore be a relation between D_2 and the network dimensionality, although the D_2 values do not give a direct measure of that dimensionality. In comparison, the data sets for the oxide glasses do not appear to show any systematic dependence of D_2 on the network dimensionality. For example, B_2O_3 and SiO_2 have 2-D and 3-D structures, respectively, but the k_2/k_2^0 ratio remains approximately invariant for both of these materials when they are initially compressed, which corresponds to a densification mechanism where the integrity of the local motifs remains unchanged as they pack more efficiently on an intermediate length scale [5]. The k_2/k_2^0 ratio then increases more rapidly as the A-O (A = B or Si) coordination number $\bar{n}_{AO}$ of these motifs starts to exceed its ambient pressure value [Fig. 2(b)].

Figure 2(c) shows the reduced-density dependence of the scaled FSDP position k_1/k_1^0 for the network-forming oxide glasses B_2O_3 [24,25], SiO_2 [26–29], and GeO_2 [30–33,35,49,50], the modified silicate glasses $CaSiO_3$ [36] and $(MgO)_{0.62}(SiO_2)_{0.38}$ [37], and the network-forming chalcogenide glasses $GeSe_2$ [38,39] and $GeSe_4$ [40,41], all under compression at ambient temperature. Also shown are the results obtained from x-ray diffraction experiments on liquid $MgSiO_3$ and $CaSiO_3$ at temperatures in the range $\simeq$1873–2390 K and pressures up to 6 GPa [51], and on molten basalt (an aluminosilicate) at temperatures in the range 2273–3273 K and pressures up to 60 GPa [52] where an estimate of k_1^0 was taken from Ref. [53]. The results for most of these materials are bracketed by curves of the form $k_1/k_1^0 = (\rho/\rho^0)^{1/D_1}$ with minimum and maximum D_1 values of 10/9 and 5/3, respectively. There appears to be no systematic dependence of D_1 on the network dimensionality. Indeed, the k_1/k_1^0 ratio can be used to give a rough estimate of ρ/ρ^0 for a wide range of materials.

III. FSDP VERSUS OXYGEN PACKING FRACTION

The results of Sec. II invite the question as to whether there is a means for rationalizing the behavior of the peak positions in $S(k)$ for disordered network-forming systems under high-pressure conditions. In particular, is there any generic feature that can be used as a fingerprint for structural change? In the case of oxides, the oxygen-packing fraction η_O is found to play a key role in determining when changes will occur to the coordination number $\bar{n}_{AO}$ of local motifs [4]. These alterations transform the network connectivity, and thereby trigger changes to physical properties such as the network compressibility [52] and viscosity [3]. In glassy SiO_2 and GeO_2, for example, the pressure-driven departure from a tetrahedral network starts to occur when $\eta_O \simeq 0.58$, which falls within the range of values found for a random loose-packing of hard spheres, and the transformation to an octahedral network is largely completed for a compression at which $\eta_O \simeq 0.64$, the value found for a random close-packed arrangement of hard spheres [4]. In glassy B_2O_3, the ambient pressure value $\bar{n}_{BO} = 3$ is first exceeded for a compression at which $\eta_O \simeq 0.44$ [4]. The oxygen-packing fraction is therefore a likely candidate for identifying markers of structural change.

The FSDP is a robust feature in the $S(k)$ functions measured by both x-ray and neutron diffraction, and k_1/k_1^0 shows a greater change with ρ/ρ^0 than either k_2/k_2^0 or k_3/k_3^0 (Fig. 2). But, as shown in Fig. 3(a), a plot of η_O versus k_1/k_1^0 does not show communal behavior. In this figure, the neutron and x-ray diffraction data sets correspond to the network-forming oxide glasses B_2O_3 [24,25], SiO_2 [27–29], and GeO_2 [30–33,35,49,50], to the modified silicate glasses $(MgO)_{0.62}(SiO_2)_{0.38}$ [37] and $CaSiO_3$ [36], and to molten $MgSiO_3$ and $CaSiO_3$ [51] under high-pressure and high-temperature conditions. For a network former such as AO_2 or A_2O_3, the η_O values were calculated by assuming that atoms of type A fit into the interstitial vacancies formed by spherical oxygen atoms. Then, for a system of volume V containing N_O oxygen atoms of volume V_O, $\eta_O = N_O V_O/V = \rho_O V_O$ where $\rho_O \equiv N_O/V = c_O\rho$ is the number density of oxygen atoms [4]. For a modified material, the η_O values were calculated by assuming that the space occupied by the modifier atoms M is not available to oxygen. Then, for a system containing N_M modifier atoms of volume V_M, $\eta_O = N_O V_O/(V - \sum_M N_M V_M) = \rho_O V_O/(1 - \sum_M \rho_M V_M)$ where $\rho_M \equiv N_M/V = c_M\rho$ is the number density of modifier atoms [4]. The η_O values then follow from the measured densities and modifier radii, and from oxygen radii that were taken from Ref. [4], except for the pressure range corresponding to $4 < \bar{n}_{SiO} < 6$ for the data sets from Refs. [27,28] where the pressure dependence of the oxygen radius was taken from Ref. [5]. The η_O values from Ref. [35] were taken directly from that paper.

The data sets describing the intermediate-range order do, however, fall into a distribution about a common curve if they are plotted as η_O/η_O^0 versus k_1/k_1^0 [Fig. 3(b)], provided that η_O/η_O^0 for a given material spans a range for which $\bar{n}_{AO}$ retains its ambient pressure value. The inset to this figure focuses on the data sets corresponding to these ambient-pressure $\bar{n}_{AO}$ values, and shows a communality that is insensitive to the ambient-pressure network dimensionality, e.g., 2-D for B_2O_3 versus 3-D for SiO_2 and GeO_2. Thus, the position of the FSDP in a measured diffraction pattern can be used to gauge the likely starting point at which a network's topology will start its pressure-driven transformation. For example, in the case of

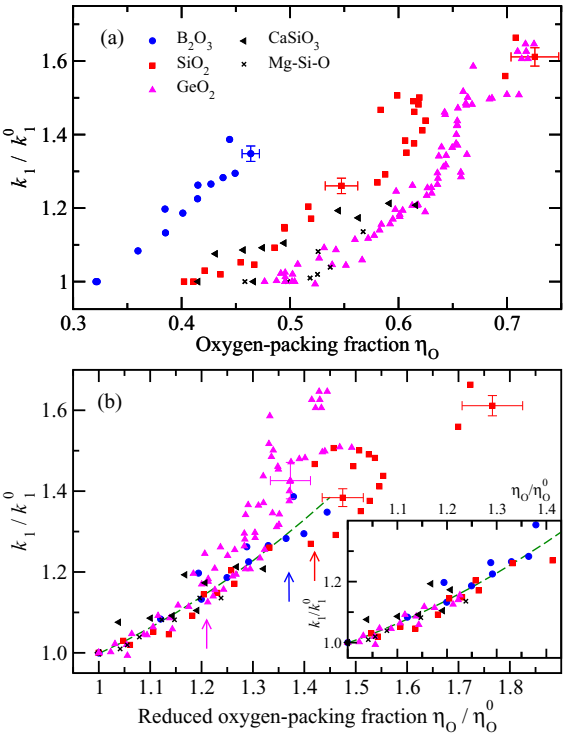

FIG. 3. The dependence of the scaled FSDP position k_1/k_1^0 on (a) the oxygen-packing fraction η_O and (b) the reduced oxygen-packing fraction η_O/η_O^0 for a variety of glassy and liquid oxides under compression. The horizontal and vertical error bars on several of the data points give representative uncertainties. In (b) the vertical arrows indicate (from left to right) the η_O/η_O^0 values at which the coordination number $\bar{n}_{AO}$ of the local motifs in glassy GeO_2, B_2O_3, and SiO_2 starts to exceed its ambient pressure value of 4, 3, or 4, respectively, and correspond to η_O values of 0.59, 0.44, and 0.58, respectively. The inset shows only those data points for which $\bar{n}_{AO}$ retains its ambient pressure value, and the broken curve (also illustrated in the main panel) shows a fit to this data.

tetrahedral networks, $\bar{n}_{AO}$ will start to exceed four when $\eta_O \simeq 0.58$ [4] and the corresponding k_1 value can be estimated from Fig. 3(b) via knowledge of the ambient-pressure parameters η_O^0 and k_1^0. We note that η_O will increase with decreasing free volume; i.e., k_1/k_1^0 will be sensitive to the reduction in this volume with increasing pressure.

The sensitivity of η_O to structural change most likely originates from an ability of the O^{2-} ion to change its size and shape in response to the coordination environment in which it is confined. For example, in molecular dynamics simulations of the structure of B_2O_3 under compression it is necessary to incorporate both of these features into an ionic interaction model [25], and in the limit when a confining potential is removed the isolated O^{2-} ion is unstable [54,55]. The chalcogen packing fraction did not provide a basis for rationalizing the pressure-dependent behavior of the peak positions in $S(k)$ from the experiments on chalcogenide glasses reported in Sec. II.

IV. CONCLUSIONS

In summary, the density-driven structural changes to disordered network-forming materials have a profound effect on their physical properties. Here, we investigated the use of pressure as a parameter to tune the density and, by analyzing the information available from *in situ* high-pressure x-ray and neutron diffraction experiments, we find that the more-open structures of network-forming materials lead to a richer variety of behavior as compared to their amorphous metallic counterparts [16]. For glassy and liquid oxides, we find that η_O provides a link between the ordering that occurs on an intermediate length scale, as described by the position of the FSDP, and the structural changes that occur on a local length scale. Thus, the FSDP provides a marker for the associated transformation of the material properties, which will prove valuable when exploring the structure-property relationships for this important class of materials, e.g., under the extreme conditions found in planetary interiors, or when preparing new glassy materials with the desired characteristics via a high-pressure processing route [4,52,56,57].

ACKNOWLEDGMENTS

We thank the EPSRC for financial support via Grant No. EP/J009741/1, and Shinya Hosokawa (Kumamoto) for the x-ray metallic glass data shown in Fig. 1. A.Z. is supported by a Royal Society–EPSRC Dorothy Hodgkin Research Fellowship.

[1] S. K. Lee, P. J. Eng, and H.-k. Mao, Rev. Mineral. Geochem. **78**, 139 (2014).
[2] D. R. Neuville, D. de Ligny, and G. S. Henderson, Rev. Mineral. Geochem. **78**, 509 (2014).
[3] Y. Wang, T. Sakamaki, L. B. Skinner, Z. Jing, T. Yu, Y. Kono, C. Park, G. Shen, M. L. Rivers, and S. R. Sutton, Nat. Commun. **5**, 3241 (2014).
[4] A. Zeidler, P. S. Salmon, and L. B. Skinner, Proc. Natl. Acad. Sci. USA **111**, 10045 (2014).
[5] P. S. Salmon and A. Zeidler, J. Phys.: Condens. Matter **27**, 133201 (2015).
[6] S. C. Moss and D. L. Price, in *Physics of Disordered Materials*, edited by D. Adler, H. Fritzsche, and S. R. Ovshinsky (Plenum, New York, 1985), p. 77.
[7] D. L. Price, S. C. Moss, R. Reijers, M.-L. Saboungi, and S. Susman, J. Phys. C: Solid State Phys. **21**, L1069 (1988).
[8] S. R. Elliott, Nature (London) **354**, 445 (1991).
[9] P. S. Salmon, Proc. R. Soc. London A **437**, 591 (1992).
[10] P. S. Salmon, Proc. R. Soc. London A **445**, 351 (1994).
[11] D. B. Miracle, Nat. Mater. **3**, 697 (2004).
[12] P. S. Salmon, R. A. Martin, P. E. Mason, and G. J. Cuello, Nature (London) **435**, 75 (2005).
[13] H. W. Sheng, W. K. Luo, F. M. Alamgir, J. M. Bai, and E. Ma, Nature (London) **439**, 419 (2006).
[14] D. Ma, A. D. Stoica, and X.-L. Wang, Nat. Mater. **8**, 30 (2009).
[15] P. S. Salmon and A. Zeidler, Phys. Chem. Chem. Phys. **15**, 15286 (2013).

[16] Q. Zeng, Y. Kono, Y. Lin, Z. Zeng, J. Wang, S. V. Sinogeikin, C. Park, Y. Meng, W. Yang, H.-K. Mao, and W. L. Mao, Phys. Rev. Lett. **112**, 185502 (2014).
[17] P. S. Salmon, J. Phys.: Condens. Matter **18**, 11443 (2006).
[18] Y. Q. Cheng and E. Ma, Prog. Mater. Sci. **56**, 379 (2011).
[19] P. Chirawatkul, A. Zeidler, P. S. Salmon, S. Takeda, Y. Kawakita, T. Usuki, and H. E. Fischer, Phys. Rev. B **83**, 014203 (2011).
[20] D. Z. Chen, C. Y. Shi, Q. An, Q. Zeng, W. L. Mao, W. A. Goddard, III, and J. R. Greer, Science **349**, 1306 (2015).
[21] R. Zallen, *The Physics of Amorphous Solids* (Wiley-VCH, Weinheim, 2004).
[22] H. E. Fischer, A. C. Barnes, and P. S. Salmon, Rep. Prog. Phys. **69**, 233 (2006).
[23] Q. Zeng, Y. Lin, Y. Liu, Z. Zeng, C. Y. Shi, B. Zhang, H. Lou, S. V. Sinogeikin, Y. Kono, C. Kenney-Benson, C. Park, W. Yang, W. Wang, H. Sheng, H.-k. Mao, and W. L. Mao, Proc. Natl. Acad. Sci. USA **113**, 1714 (2016).
[24] V. V. Brazhkin, Y. Katayama, K. Trachenko, O. B. Tsiok, A. G. Lyapin, E. Artacho, M. Dove, G. Ferlat, Y. Inamura, and H. Saitoh, Phys. Rev. Lett. **101**, 035702 (2008).
[25] A. Zeidler, K. Wezka, D. A. J. Whittaker, P. S. Salmon, A. Baroni, S. Klotz, H. E. Fischer, M. C. Wilding, C. L. Bull, M. G. Tucker, M. Salanne, G. Ferlat, and M. Micoulaut, Phys. Rev. B **90**, 024206 (2014).
[26] Y. Inamura, Y. Katayama, W. Utsumi, and K. I. Funakoshi, Phys. Rev. Lett. **93**, 015501 (2004).
[27] C. J. Benmore, E. Soignard, S. A. Amin, M. Guthrie, S. D. Shastri, P. L. Lee, and J. L. Yarger, Phys. Rev. B **81**, 054105 (2010).
[28] T. Sato and N. Funamori, Phys. Rev. B **82**, 184102 (2010).
[29] A. Zeidler, K. Wezka, R. F. Rowlands, D. A. J. Whittaker, P. S. Salmon, A. Polidori, J. W. E. Drewitt, S. Klotz, H. E. Fischer, M. C. Wilding, C. L. Bull, M. G. Tucker, and M. Wilson, Phys. Rev. Lett. **113**, 135501 (2014).
[30] Q. Mei, S. Sinogeikin, G. Shen, S. Amin, C. J. Benmore, and K. Ding, Phys. Rev. B **81**, 174113 (2010).
[31] J. W. E. Drewitt, P. S. Salmon, A. C. Barnes, S. Klotz, H. E. Fischer, and W. A. Crichton, Phys. Rev. B **81**, 014202 (2010).
[32] P. S. Salmon, J. W. E. Drewitt, D. A. J. Whittaker, A. Zeidler, K. Wezka, C. L. Bull, M. G. Tucker, M. C. Wilding, M. Guthrie, and D. Marrocchelli, J. Phys.: Condens. Matter **24**, 415102 (2012).
[33] K. Wezka, P. S. Salmon, A. Zeidler, D. A. J. Whittaker, J. W. E. Drewitt, S. Klotz, H. E. Fischer, and D. Marrocchelli, J. Phys.: Condens. Matter **24**, 502101 (2012).
[34] X. Hong, L. Ehm, and T. S. Duffy, Appl. Phys. Lett. **105**, 081904 (2014).
[35] Y. Kono, C. Kenney-Benson, D. Ikuta, Y. Shibazaki, Y. Wang, and G. Shen, Proc. Natl. Acad. Sci. USA **113**, 3436 (2016).
[36] K. J. Pizzey, Ph.D. thesis, University of Bath, UK, 2015.
[37] M. Wilding, M. Guthrie, S. Kohara, C. L. Bull, J. Akola, and M. G. Tucker, J. Phys.: Condens. Matter **24**, 225403 (2012).
[38] Q. Mei, C. J. Benmore, R. T. Hart, E. Bychkov, P. S. Salmon, C. D. Martin, F. M. Michel, S. M. Antao, P. J. Chupus, P. L. Lee, S. D. Shastri, J. B. Parise, K. Leinenweber, S. Amin, and J. L. Yarger, Phys. Rev. B **74**, 014203 (2006).
[39] K. Wezka, A. Bouzid, K. J. Pizzey, P. S. Salmon, A. Zeidler, S. Klotz, H. E. Fischer, C. L. Bull, M. G. Tucker, M. Boero, S. Le Roux, C. Tugène, and C. Massobrio, Phys. Rev. B **90**, 054206 (2014).
[40] L. B. Skinner, C. J. Benmore, S. Antao, E. Soignard, S. A. Amin, E. Bychkov, E. Rissi, J. B. Parise, and J. L. Yarger, J. Phys. Chem. C **116**, 2212 (2012).
[41] B. Kalkan, R. P. Dias, C.-S. Yoo, S. M. Clark, and S. Sen, J. Phys. Chem. C **118**, 5110 (2014).
[42] A. Bouzid, K. J. Pizzey, A. Zeidler, G. Ori, M. Boero, C. Massobrio, S. Klotz, H. E. Fischer, C. L. Bull, and P. S. Salmon, Phys. Rev. B **93**, 014202 (2016).
[43] K. Tanaka, Phys. Rev. B **42**, 11245 (1990).
[44] Y. Akahama, M. Kobayashi, and H. Kawamura, Phys. Rev. B **56**, 5027 (1997).
[45] K. Yang, Q. Cui, Y. Hou, B. Liu, Q. Zhou, J. Hu, H.-k. Mao, and G. Zou, J. Phys.: Condens. Matter **19**, 425220 (2007).
[46] H. Liu, L. Wang, X. Xiao, F. De Carlo, J. Feng, H.-k. Mao, and R. J. Hemley, Proc. Natl. Acad. Sci. USA **105**, 13229 (2008).
[47] Q. Mei, C. J. Benmore, S. Sen, R. Sharma, and J. L. Yarger, Phys. Rev. B **78**, 144204 (2008).
[48] B. A. Weinstein, R. Zallen, M. L. Slade, and J. C. Mikkelsen, Jr., Phys. Rev. B **25**, 781 (1982).
[49] M. Guthrie, C. A. Tulk, C. J. Benmore, J. Xu, J. L. Yarger, D. D. Klug, J. S. Tse, H.-k. Mao, and R. J. Hemley, Phys. Rev. Lett. **93**, 115502 (2004).
[50] X. Hong, G. Shen, V. B. Prakapenka, M. Newville, M. L. Rivers, and S. R. Sutton, Phys. Rev. B **75**, 104201 (2007).
[51] N. Funamori, S. Yamamoto, T. Yagi, and T. Kikegawa, J. Geophys. Res. **109**, B03203 (2004).
[52] C. Sanloup, J. W. E. Drewitt, Z. Konôpková, P. Dalladay-Simpson, D. M. Morton, N. Rai, W. van Westrenen, and W. Morgenroth, Nature (London) **503**, 104 (2013).
[53] J. W. E. Drewitt, C. Sanloup, A. Bytchkov, S. Brassamin, and L. Hennet, Phys. Rev. B **87**, 224201 (2013).
[54] M. Tokonami, Acta Cryst. **19**, 486 (1965).
[55] P. Jemmer, P. W. Fowler, M. Wilson, and P. A. Madden, J. Phys. Chem. A **102**, 8377 (1998).
[56] M. M. Smedskjaer, R. E. Youngman, S. Striepe, M. Potuzak, U. Bauer, J. Deubener, H. Behrens, J. C. Mauro, and Y. Yue, Sci. Rep. **4**, 3770 (2014).
[57] M. M. Smedskjaer, S. J. Rzoska, M. Bockowski, and J. C. Mauro, J. Chem. Phys. **140**, 054511 (2014).